Available online at www.synsint.com

Synthesis and Sintering

ISSN 2564-0186 (Print), **ISSN** 2564-0194 (Online)

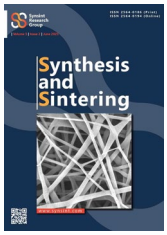

Research article

Effect of ZnO nanoparticles on the dielectric and magnetic behavior of bismuth ferrite ceramics

Fatemeh Pourbagher, Hajar Ahmadimoghadam *, Ibrahim Sharifi

Materials Engineering Department, Faculty of Engineering, Shahrekord University, Shahrekord, Iran

A B S T R A C T

Bismuth ferrite ($BiFeO_3$, BFO) is a promising multiferroic material due to its inherent ferroelectric and antiferromagnetic properties; however, its practical applications are limited by weak dielectric and magnetic performance, as well as challenges in achieving pure-phase synthesis. In this study, the effects of incorporating zinc oxide (ZnO) nanoparticles at 0.5, 1, and 2 wt% on the dielectric and magnetic properties of BFO ceramics were systematically investigated. X-ray diffraction analysis confirmed that the addition of ZnO suppressed the formation of secondary phases and enhanced phase purity. A notable increase in relative density (from 94.3% to 98.2%) and a corresponding reduction in porosity were observed with increasing ZnO content. The dielectric constant significantly improved from 450 (pure BFO) to 4900 (2 wt% ZnO) at 1 kHz, albeit accompanied by a moderate rise in dielectric loss. Magnetic measurements revealed an increase in saturation magnetization from 0.18 to 0.44 emu/g and a decrease in coercivity from 810 to 560 Oe. These enhancements are attributed to the reduction of non-magnetic secondary phases, improved densification, and structural modifications induced by ZnO incorporation. Overall, the addition of ZnO presents an effective strategy for enhancing the multifunctional performance of BFO ceramics, making them more viable for advanced device applications.

K E Y W O R D S

Bismuth ferrite
ZnO nanoparticles
Density
Dielectric properties
Magnetic properties

OPEN ACCESS

1. Introduction

Bismuth ferrite ($BiFeO_3$, BFO) is a rare single-phase multiferroic ceramic that exhibits both ferroelectric and antiferromagnetic properties at room temperature. Its rhombohedral perovskite (ABO_3) structure supports simultaneous spin ordering and spontaneous electric polarization, wherein Bi^{3+} ions occupy the A-sites, inducing ferroelectricity through $6s^2$ lone pairs, and Fe^{3+} ions at the B-sites contribute to antiferromagnetism. Over the past decades, BFO has attracted substantial research attention due to its strong ferroelectric polarization, high Curie temperature (~1103 K), and antiferromagnetic Néel temperature (~653 K), making it a promising candidate for applications in memory devices, sensors, actuators, and microwave absorbers [1–4].

Despite its multifunctionality, BFO suffers from intrinsic limitations, including high leakage current, weak magnetic response, and relatively low dielectric performance. A major challenge in BFO synthesis is the formation of secondary phases (e.g., Bi_2O_3, Fe_2O_3, $Bi_{25}FeO_{40}$), which adversely affect its electrical and magnetic properties [5–7]. Various strategies have been proposed to overcome these drawbacks, such as cation substitution at A- or B-sites, doping, solid solution formation, and composite design [8–10]. Incorporating ABO_3-type compounds—such as $BaTiO_3$, $PbTiO_3$, $SrTiO_3$, or $NaNbO_3$—into the BFO matrix has been shown to substantially improve structural stability and functional properties [11]. For instance, Qian et al. [12] synthesized (1-x)$BiFeO_3$–x($SrTiO_3$–$Bi_{0.5}Na_{0.5}TiO_3$) solid solutions and reported enhanced ferroelectric performance.

* Corresponding author. *E-mail address:* hajar.ahmadi@sku.ac.ir (H. Ahmadimoghadam)
Received 26 April 2025; Received in revised form 24 May 2025; Accepted 25 May 2025.

https://doi.org/10.53063/synsint.2025.52286

A-site doping influences ferroelectric properties primarily through FeO_6 octahedral distortion and oxygen vacancy formation, while B-site doping modifies magnetic behavior by disrupting spin cycloids or exchange interactions. For example, Sm doping at the A-site significantly improved the electrical performance of BFO, as demonstrated by Singh et al. [13]. Wang et al. [14] employed rapid liquid-phase sintering to achieve a remanent polarization of 0.4 μC/cm², attributed to reduced oxygen vacancies and Fe^{2+} content. Moreover, the incorporation of $45BaO–32TiO_2–23SiO_2$ (BTS) glass into BFO enhanced dielectric breakdown strength, thermal stability, and fatigue resistance by forming an insulating glassy network that suppressed leakage currents [15].

Recent studies have also explored Zn-based modifications. Zn doping has been reported to reduce secondary phase formation, improve densification, and enhance dielectric and magnetic properties [16–18]. Co-doping with Zn and Ti improved polarization and reduced dielectric losses [19]. Additionally, the incorporation of ZnO in composite systems, such as in $Bi_{0.99}Nd_{0.01}FeO_3$ ceramics, led to an improvement in dielectric constant and polarization at low frequencies. However, a slight increase in dielectric loss was also observed due to enhanced conductivity and modified charge dynamics [20].

While doping strategies have been extensively explored in multiferroic ceramics, research focusing on the application of metal oxide additives remains comparatively scarce. One notable study investigated the effects of various oxide additives, including Bi_2O_3, MnO_2, La_2O_3, Sm_2O_3, SnO_2, and Nb_2O_5, on the structural and electrical properties of $0.70Bi_{1.05}FeO_3–0.30BaTiO_3$ ceramics. The findings revealed that both the type and concentration of the oxide additive significantly influenced the microstructure and functional characteristics. Notably, Nb_2O_5 facilitated considerable grain refinement while suppressing the dielectric response, whereas the incorporation of SnO_2 resulted in increased magnetization attributed to lattice distortion and disruption of the spin helix structure [21].

In contrast to conventional doping, which involves the direct substitution of cationic species into lattice sites, additives can interact with the matrix during the sintering process, thereby affecting phase composition, microstructure, and functional properties without necessarily occupying specific lattice positions. The utilization of additives presents various advantages, including simplified processing, enhanced control over grain boundary behavior, and tunable effects that depend on particle size and distribution.

As previously mentioned, various zinc-based strategies—such as doping and composite formation—have demonstrated promising effects on $BiFeO_3$ ceramics by enhancing phase purity, densification, and multifunctional properties. Zinc oxide (ZnO) nanoparticles are particularly noteworthy as an additive due to their availability, cost-effectiveness, and ease of processing. Prior research has indicated that ZnO improves the dielectric properties of ceramics such as $BaTiO_3$ and $(K_{0.5}Na_{0.5})NbO_3$ by enhancing densification and reducing structural defects [22, 23].

Nonetheless, investigations utilizing ZnO as a standalone additive—rather than as a dopant or composite component—remain remarkably limited. Inspired by the promising outcomes associated with other oxide additives, the present study aims to examine the effects of directly incorporating ZnO nanoparticles into $BiFeO_3$ ceramics synthesized via a conventional solid-state route. This additive-based approach provides a structurally non-invasive and scalable methodology for exploring potential modifications in the dielectric and magnetic properties of $BiFeO_3$ ceramics.

2. Experimental procedures

Bismuth ferrite (BFO) powder was synthesized using the conventional solid-state reaction method with high-purity oxides: bismuth oxide (Bi_2O_3, 99% purity, Merck) and iron oxide (Fe_2O_3, 99.5% purity, Merck). Zinc oxide (ZnO) nanoparticles (99.9% purity, <80 nm particle size) were added as an additive. Stoichiometric amounts of Bi_2O_3 and Fe_2O_3 were mixed using high-energy planetary ball milling at 150 rpm for 4 h, with a ball-to-powder weight ratio of 20:1 in an ethanol medium. The resulting slurry was dried at 90 °C for 12 h and then calcined at 750 °C for 2 h in an electric furnace, with a heating rate of 5 °C/min. The calcined BFO powder was mixed with ZnO nanoparticles in different weight percentages (0.5, 1, and 2 wt%) using the same milling parameters. The mixed powders were uniaxially pressed into disk-shaped pellets (15 mm in diameter) under a pressure of 150 MPa, followed by sintering at 850 °C for 2 h with a heating rate of 5 °C/min. The samples were labeled as BFO (undoped), BFO-0.5Z, BFO-1Z, and BFO-2Z, corresponding to 0.5, 1, and 2 wt% ZnO addition, respectively.

Phase analysis was performed using X-ray diffraction (XRD, Asenware AW-XDM 300) with Cu-Kα radiation (λ = 1.5418 Å) and a step size of 0.02 °. Microstructural features, including grain size and morphology, were characterized by scanning electron microscopy (SEM, VEGA3, Tescan). The bulk density of the sintered samples was measured using the Archimedes method (ASTM C373), and the total porosity was calculated using Eq. 1, where ρ_S is the measured density and ρ_{Th} is the theoretical density (8.34 g/cm³, based on crystallographic data from standard references):

$$\text{Total porosity (\%)} = (1 - \rho S/\rho Th) \times 100 \quad (1)$$

Dielectric properties, including dielectric constant and dielectric loss (tan δ), were evaluated at room temperature across a frequency range of 50 Hz to 100 kHz using an LCR meter (OCT1010). Magnetic hysteresis loops were obtained using a vibrating sample magnetometer (VSM, MDKB). For dielectric and magnetic measurements, silver paste was applied to both surfaces of the pellets using a brush and fired at 400 °C for 15 min to ensure good electrical contact.

3. Results and discussion

3.1. XRD analysis and phase identification

Fig. 1 displays the X-ray diffraction (XRD) patterns of $BiFeO_3$ ceramics with varying weight percentages of ZnO nanoparticles. Phase analysis conducted using High Score Plus software identified three crystalline phases: $BiFeO_3$ (BFO), sillenite-type $Bi_{25}FeO_{40}$, and Bi_2O_3. The observed diffraction peaks confirm the presence of a rhombohedral perovskite structure consistent with JCPDS card no. 96-210-2916, with characteristic reflections from the (012), (104), (110), (006), (202), and (024) planes.

As mentioned in the introduction, achieving phase-pure BFO is difficult due to the volatility of bismuth at high temperatures and the limited diffusion of Fe ions into the Bi_2O_3 matrix. These conditions can result in incomplete reactions and the formation of secondary phases [2, 24]. The diffraction peaks corresponding to $Bi_{25}FeO_{40}$ match the

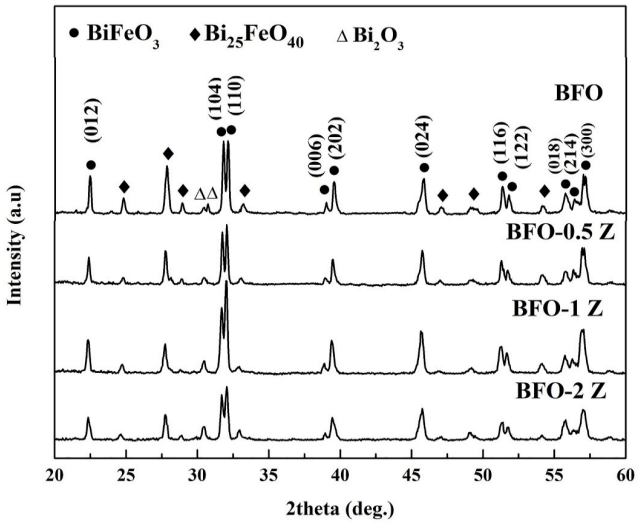

Fig. 1. XRD patterns of bismuth ferrite ceramics with varying wt% of ZnO nanoparticles.

JCPDS card no. 96-901-1269 (cubic structure), while those of Bi_2O_3 align with JCPDS card no. 96-101-0314 (cubic structure).

With the addition of ZnO nanoparticles, the intensity of secondary phase peaks decreased, indicating improved phase purity in the BFO matrix [17]. This improvement may stem from surface interactions between ZnO nanoparticles and the secondary phases, disrupting the stability of impurity phases and promoting the formation of the primary perovskite structure. ZnO may also play a kinetic role during thermal treatment, preventing the overgrowth of secondary phases and facilitating a more uniform and well-crystallized BFO phase [25].

The lack of distinct diffraction peaks associated with ZnO in the XRD patterns may be due to the low ZnO content or the potential incorporation of Zn^{2+} ions into the BFO crystal lattice or their presence in an amorphous form, both below the detection limit of XRD

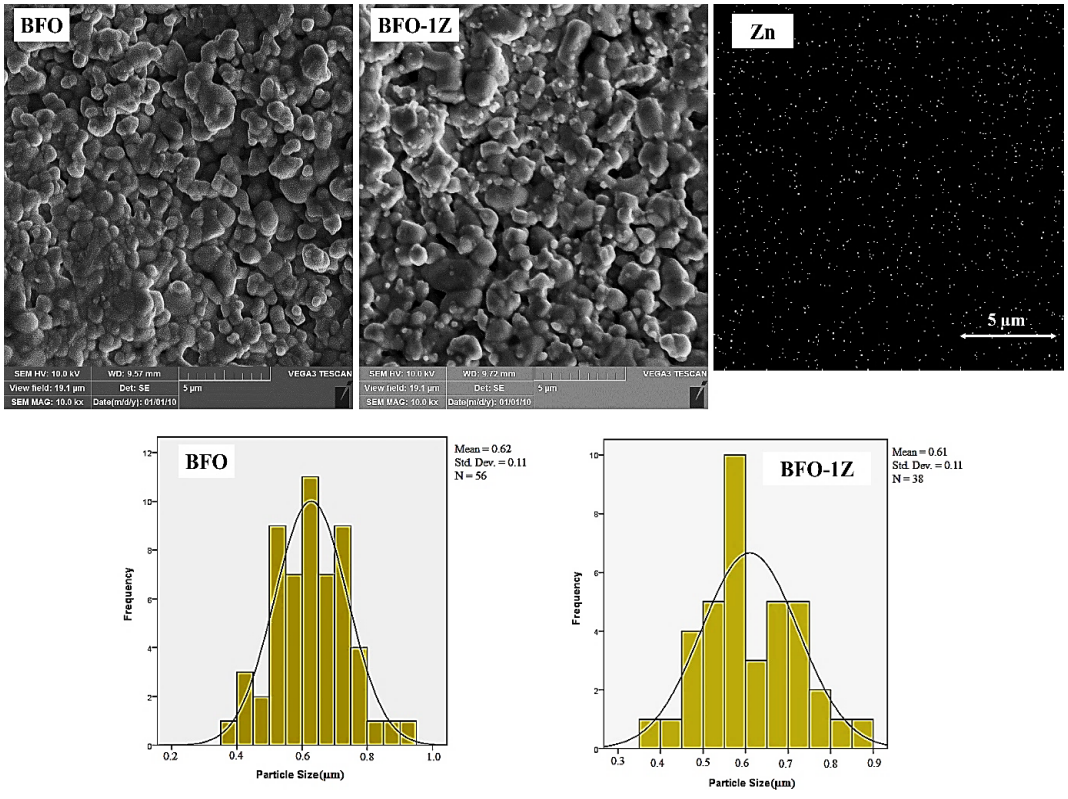

Fig. 2. SEM images of the fracture surfaces of BFO and BFO-1Z samples, accompanied by statistical grain-size distribution analysis.

Table 1. Density, relative density, and total porosity of the samples.

Sample	Density (g/cm³)	Relative density (%)	Total porosity (%)
BFO	7.86	94.3	5.7
BFO-0.5 Z	8.06	96.6	3.4
BFO-1 Z	8.15	97.7	2.3
BFO-2 Z	8.19	98.2	1.8

analysis. Furthermore, the absence of any new impurity phase supports the idea that Zn contributes to the stabilization of the perovskite structure [4, 7, 20].

No significant shift in peak positions was observed with increasing ZnO content, indicating that any potential substitution of Fe^{3+} with Zn^{2+} did not significantly alter the lattice parameters. This lack of change could be attributed to the close similarity between the ionic radii of Zn^{2+} (0.74 Å) and Fe^{3+} (0.78 Å) [18].

3.2. Microstructural analysis and densification

Fig. 2 presents SEM images of the fracture surfaces of the BFO and BFO-1Z samples, along with the statistical analysis of their grain size distribution. Both samples show relatively homogeneous morphologies with interconnected, quasi-spherical grains. However, the BFO-1Z sample exhibits a denser and more uniform microstructure compared to the undoped BFO. This difference can be attributed to the role of ZnO in promoting grain growth and structural coherence during the sintering process. Due to their high surface energy and reactivity at the nanoscale, ZnO nanoparticles may act as sintering aids, enhancing grain mobility and filling voids more effectively during densification [25]. Although distinct peaks corresponding to ZnO were not observed in the XRD patterns, this absence is likely attributable to the low ZnO content (0.5–2 wt%), which may fall below the detection limit of conventional XRD techniques. To further elucidate the distribution of zinc, elemental mapping was performed. As illustrated in Fig. 2, zinc is relatively uniformly distributed throughout the microstructure, with a slight propensity to accumulate at grain boundaries. These findings suggest that ZnO does not form a separate crystalline phase detectable by XRD and may instead be preferentially localized at grain interfaces [21, 22].

The average grain sizes for the BFO and BFO-1Z samples were measured to be 0.62 µm and 0.61 µm, respectively, indicating negligible differences in grain size [20]. However, the BFO-1Z sample showed a slightly narrower and more symmetric grain size distribution, with an identical standard deviation of 0.11 µm reported for both samples.

Table 1 summarizes the results of bulk density and porosity measurements. One of the key challenges in sintering ceramics containing volatile components such as bismuth is achieving high densification. This is because high vapor pressure elements tend to evaporate at elevated temperatures, which becomes more pronounced as the temperature increases [7]. The bulk density of the pure BFO sample was found to be 7.86 g/cm³, which corresponds to 94.3% of the

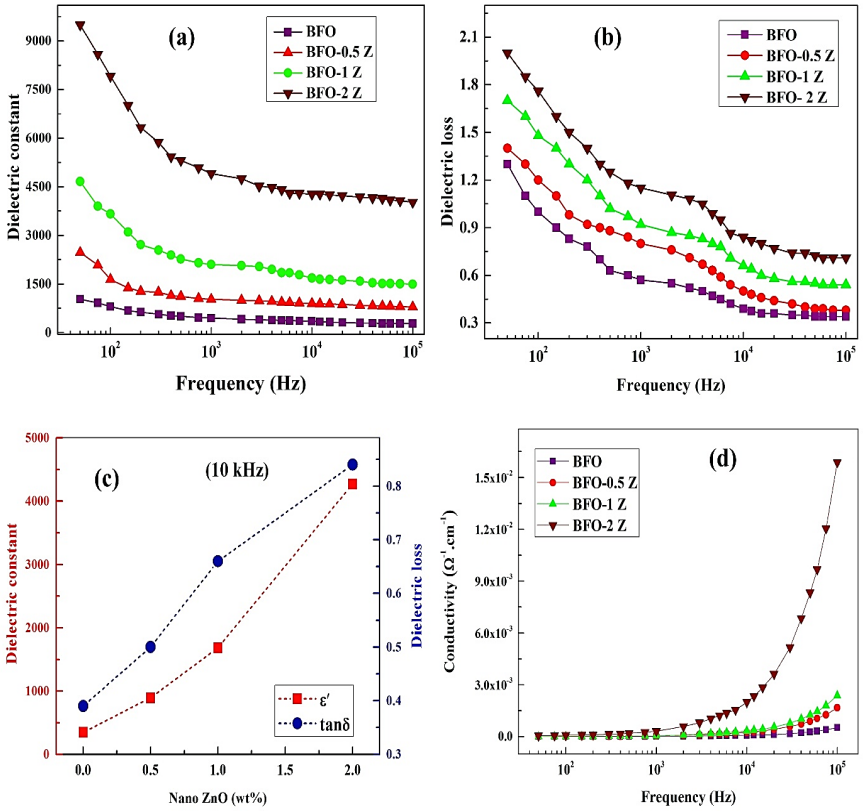

Fig. 3. a) Variation of the dielectric constant, b) dielectric loss of the samples as a function of frequency, c) values of the dielectric constant and dielectric loss of the samples measured at 10 kHz, and d) variation of the AC conductivity of the samples as a function of frequency.

theoretical density (8.34 g/cm³), with a total porosity of approximately 7.5%. The addition of ZnO nanoparticles significantly improved the densification behavior of the BFO ceramics. As the ZnO content increased, the relative density steadily increased, reaching a maximum of 98.2% in the BFO-2Z sample. This trend highlights the positive effect of ZnO as a sintering aid, enhancing compactability and promoting a more homogeneous microstructure in the ceramics.

3.3. Dielectric properties and frequency-dependent behavior

The dielectric constant and dielectric loss of the samples as a function of frequency are shown in Fig. 3. Additionally, Fig. 3c displays the values of the dielectric constant and dielectric loss of the samples at a frequency of 10 kHz. The graphs of dielectric constant (ε) and dielectric loss (tan δ) illustrate a decrease in both parameters with increasing frequency. This behavior is due to the frequency-dependent nature of the polarization mechanisms. At lower frequencies (up to 10^3 Hz), all polarization mechanisms, including space charge, dipole, ionic, and electronic polarization, contribute to the dielectric constant. However, as the frequency increases, slower mechanisms such as space charge and dipole polarization are unable to keep pace with the rapid changes in the electric field. This leads to a decrease in their contribution, subsequently resulting in a reduction in the dielectric constant.

Regarding dielectric loss (tan δ), at lower frequencies, mechanisms such as ionic conductivity and dipole relaxation contribute significantly to energy dissipation. As the frequency increases, these mechanisms become less effective, as the material cannot respond rapidly enough to the changing electric field, resulting in a decrease in tan δ. This trend is observed consistently across all samples and is characteristic of typical dielectric material behavior [4, 19, 24].

The pure BFO sample exhibits the lowest dielectric constant across all frequencies, ranging from approximately 300 to 1000. Upon adding 0.5% ZnO, the dielectric constant increases to around 1000 to 2500 at lower frequencies. When the ZnO content is increased to 1%, there is a significant increase in the dielectric constant, reaching around 4500 at lower frequencies. The highest dielectric constant values, approximately 9000 at lower frequencies, are observed for the BFO-2Z sample; however, there is a sharp decrease with increasing frequency. As shown in Fig. 3c, with the increase of ZnO content up to 2 wt%, the dielectric constant rises from 490 to 4900, and the dielectric loss increases from 0.4 to 0.8. The addition of nano-sized ZnO enhances the dielectric constant of the $BiFeO_3$ ceramics, particularly at lower frequencies. This increase is likely due to the improvement in space charge polarization or the increase in structural defects, such as oxygen vacancies, introduced with the addition of ZnO. The possible substitution of Fe^{3+} ions by Zn^{2+} ions and the formation of complex defects could increase the space charge polarization. These defects arise due to ion substitution or changes in the crystal lattice, both of which enhance the dielectric constant [19].

Moreover, the reduction of the secondary $Bi_{25}FeO_{40}$ phase upon adding ZnO may also contribute to the improvement of the dielectric constant [17]. SEM images show that the BFO-1Z sample exhibits more aggregated particles. This aggregation, along with a narrower particle size distribution, may increase the surface area and interfacial contact, which can lead to an enhancement in both dielectric constant and loss. The addition of ZnO may strengthen the dipolar or ionic polarization mechanisms, which are more effective at lower frequencies, thus increasing in the dielectric constant [16, 18].

However, the increase in dielectric loss may be attributed to the increased ionic conductivity associated with the defects introduced by ZnO. The addition of nano-ZnO significantly increases dielectric loss, especially at lower frequencies. This increase may be due to the enhanced structural defects or ionic conduction caused by ZnO. At higher frequencies, however, the dielectric loss for all samples converges to similar values. It is often observed that materials with high dielectric constants also exhibit higher dielectric losses. Furthermore, materials with complex structures have different polarization mechanisms, which also lead to higher dielectric loss. Therefore, the increase in dielectric loss in the ZnO-containing samples can also be attributed to the enhancement in their dielectric constant [16, 20].

The significant increase in dielectric constant observed with the addition of ZnO highlights the potential of this additive strategy for improving the dielectric response of bismuth ferrite (BFO) ceramics. While the dielectric loss of 0.8 at 10 kHz may still be acceptable for certain sensor applications, it could limit performance in high-frequency capacitor applications, necessitating further optimization. However, the concomitant moderate rise in dielectric loss, particularly at elevated frequencies, suggests a possible enhancement in electrical conductivity or defect-assisted charge transport mechanisms. This trade-off between dielectric enhancement and increased loss requires careful consideration for practical applications. Future research could focus on optimizing ZnO content, refining sintering conditions to mitigate defect formation, or incorporating co-additives that effectively suppress leakage currents while maintaining low loss and high dielectric performance.

3.4. AC electrical conductivity

The alternating current conductivity (σ_{ac}) of the samples was calculated using the following Eq. 2, where ε_0 is the permittivity of free space, and $\omega = 2\pi f$ is the angular frequency [16]. The results for the variation of σ_ac with frequency, obtained using this equation, are shown in Fig. 3d. At low frequencies, the conductivity remains almost constant and independent of frequency, reflecting the direct current conductivity (σ_{dc}) of the samples. After reaching a specific frequency (known as the hopping frequency or percolation frequency), the AC conductivity increases rapidly. This behavior is consistent with the power law model (Eq. 3):

$$\sigma_{ac}=\varepsilon 0\varepsilon'\omega\tan\delta \quad (2)$$

$$\sigma_{ac}=\sigma_{dc}+A\omega n \quad (3)$$

In these equations, A represents a temperature-related coefficient associated with the polarization and stability of the polarization, while n describes the interaction between the ions and the crystal lattice in the ceramic material [4, 7]. As depicted in Fig. 3d, the introduction of nano zinc oxide (ZnO) results in enhanced electrical conductivity in the BFO-Z samples, particularly in the BFO-2Z sample, in comparison to the pure BFO sample. This enhancement is most prominent at higher frequencies. The reasons for this increase are as follows:

- The presence of ZnO at the grain boundaries can lead to an increase in the dielectric constant (ε′) due to the high polarization of these nanoparticles, resulting in higher energy storage capacity in the sample. As per Eq. 2, a higher dielectric constant (ε′) corresponds to a higher σ_{ac}.

Table 2. AC conductivity parameters and magnetic properties of the samples.

Sample	σ_{dc} $(\Omega \cdot m)^{-1}$	n	A $(\Omega \cdot m)^{-1}$	R^2	M_r (emu/g)	M_s (emu/g)	H_c (Oe)
BFO	3×10^{-6}	0.670	2×10^{-7}	0.992	0.020	0.18	810
BFO-0.5 Z	8×10^{-6}	0.711	4×10^{-7}	0.997	0.028	0.25	640
BFO-1 Z	1×10^{-5}	0.730	6×10^{-7}	0.994	0.041	0.39	640
BFO-2 Z	5×10^{-5}	0.765	2×10^{-6}	0.996	0.038	0.44	560

- The presence of ZnO nanoparticles also causes an increase in dielectric loss (tan δ) and enhances polarization at the grain boundaries. This facilitates the movement of charge carriers, leading to an increase in AC conductivity at higher frequencies. According to Eq. 2, a higher dielectric loss (tan δ) corresponds to a higher σ_{ac} [20].
- The addition of nano ZnO in the samples results in an increase in density and a reduction in porosity. This leads to improved structural continuity and reduced barriers to conductivity. Furthermore, the inclusion of ZnO causes a decrease in the intensity of secondary phases like $Bi_{25}FeO_{40}$, shifting the samples towards a purer $BiFeO_3$ phase [17].

Table 2 displays the values of σdc, A, and n that were obtained by fitting Eq. 3 to the data shown in Fig. 3d. It also includes the correlation coefficient (R^2). High R^2 values indicate the model accurately and reliably describes the electrical behavior of the samples. Moreover, the higher values of A and n in the samples containing nano zinc oxide may indicate increased polarization and enhanced stability of polarization in these samples [4].

3.5. Magnetic hysteresis behavior

The magnetic hysteresis loops of the samples at room temperature are presented in Fig. 4, and the key magnetic parameters—remanent magnetization (M_r), saturation magnetization (M_s), and coercive field (H_c)—are summarized in Table 2. The pure BFO sample exhibits weak magnetic behavior, characterized by relatively high coercivity (810 Oe) and low magnetization values (M_s = 0.18 emu/g), indicative of its semi-hard magnetic nature. This weak response originates from the intrinsic antiferromagnetic ordering of BFO, associated with its cycloidal spin structure, where magnetic moments are arranged in a spiral and antiparallel fashion, thereby suppressing net magnetization [5].

Upon the addition of ZnO nanoparticles, notable modifications in magnetic properties are observed. The saturation magnetization (M_s) increases from 0.18 emu/g for pure BFO to 0.44 emu/g for BFO-2Z, while the coercivity (H_c) decreases from 810 Oe to 560 Oe. The remanent magnetization (M_r) also shows a slight increase. The enhancement in M_s suggests improved ferromagnetic behavior, likely due to the suppression of non-magnetic secondary phases and reinforcement of magnetic exchange interactions within the BFO matrix [17].

Furthermore, the increase in M_r reflects better domain stability, which can be associated with structural modifications and a reduction in non-magnetic defect density. Overall, the significant improvements in soft magnetic properties, especially in the BFO-1Z and BFO-2Z samples, can be attributed to several factors:

- Reduction of Non-Magnetic Secondary Phases: The incorporation of ZnO promotes enhanced sintering and improves phase purity, thereby minimizing the presence of secondary non-magnetic phases such as $Bi_{25}FeO_{40}$, which can otherwise degrade magnetic properties [17].
- Structural Distortion and Suppression of Cycloidal Spin Modulation: ZnO nanoparticles at the grain boundaries induce structural distortions that disrupt the cycloidal spin structure, allowing for greater alignment of magnetic moments under an

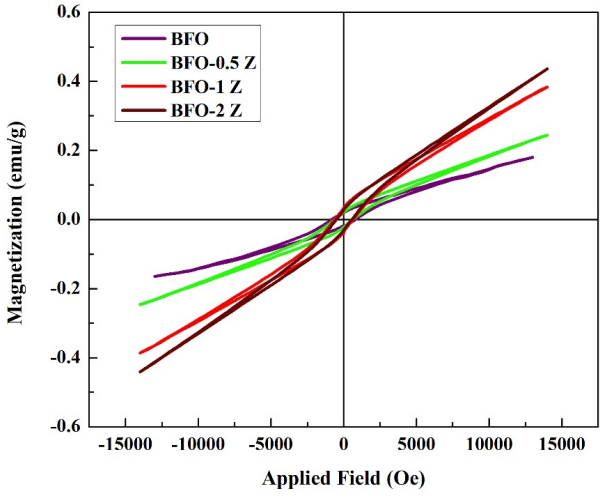

Fig. 4. Magnetic hysteresis loops of BFO samples with varying contents of ZnO nanoparticles.

external magnetic field, resulting in increased net magnetization [26].

- Improved Densification and Reduced Porosity: The enhanced density and lower porosity of ZnO-added samples lead to stronger intergranular magnetic interactions, contributing to the overall magnetic enhancement.
- Formation of New Magnetic Interactions: ZnO nanoparticles at grain boundaries may create additional magnetic interactions, modifying the magnetic permeability and dynamic response of the ceramic matrix [20].

In conclusion, the observed increase in magnetization with ZnO incorporation, particularly in the BFO-2Z sample, demonstrates the effectiveness of ZnO nanoparticles in modifying the magnetic structure and enhancing the magnetic performance of $BiFeO_3$ ceramics. The observed enhancement in saturation magnetization and the concomitant reduction in coercivity with increasing ZnO content suggest a partial suppression of the inherent spiral spin cycloid structure of bismuth ferrite. This disruption is likely facilitated by localized lattice distortions and the suppression of non-magnetic secondary phases. Similar enhancements have been documented in other oxide-modified bismuth ferrite systems, where structural inhomogeneity or chemical pressure disrupts long-range antiferromagnetic ordering, thereby enabling the emergence of uncompensated spin moments [21, 26, 27].

4. Conclusions

The incorporation of ZnO nanoparticles into bismuth ferrite ($BiFeO_3$) markedly enhanced its structural, dielectric, and magnetic properties. Phase analysis confirmed that the addition of ZnO effectively suppressed the formation of the secondary $Bi_{25}FeO_{40}$ phase and stabilized the perovskite BFO structure, thereby improving phase purity. The observed increase in relative density (up to 98.2%) and corresponding reduction in porosity (down to 1.8%) are attributed to the sintering aid effect of ZnO nanoparticles, resulting in a denser microstructure.

Regarding dielectric performance, a substantial enhancement in the dielectric constant (up to 9000 at low frequencies) was achieved, primarily due to improved space charge polarization and decreased porosity. However, this improvement was accompanied by a moderate increase in dielectric loss, likely resulting from enhanced ionic conductivity and interfacial polarization.

From a magnetic perspective, the increase in saturation magnetization and the decrease in coercivity indicate a transition toward softer magnetic behavior, which is advantageous for multifunctional applications. These improvements are mainly associated with the suppression of non-magnetic phases, structural distortion disrupting the antiferromagnetic spin structure, and enhanced domain dynamics facilitated by ZnO incorporation.

In summary, the introduction of ZnO nanoparticles presents an effective approach to optimizing the multifunctional performance of $BiFeO_3$ ceramics, making them more promising candidates for advanced multiferroic and spintronic device applications.

CRediT authorship contribution statement

Fatemeh Pourbagher: Investigation, Conceptualization, Methodology, Writing – Original Draft, Visualization.

Hajar Ahmadimoghadam: Supervision, Conceptualization, Methodology, Investigation, Data curation, Software, Project administration, Writing—original draft preparation, Writing—review and editing.

Ibrahim Sharifi: Supervision, Methodology, Conceptualization, Investigation, Writing—review and editing.

Data availability

The data underlying this article will be shared on reasonable request to the corresponding author.

Declaration of competing interest

The authors declare no competing interests.

Funding and acknowledgment

This research received no external funding. The authors have no acknowledgments to declare.

References

[1] A. Jain, Y.G. Wang, A. Kumar, N. Gupta, K. Kumar, A.K. Goyal, BiFeO3-based lead-free materials: Recent breakthroughs and their multifunctional applications, J. Alloys Compd. 1010 (2024) 177170. https://doi.org/10.1016/j.jallcom.2024.177170.

[2] A. Ahad, T. Ahamed, M.B. Biswas, E. Khandaker, A. Barik, M.A. Taher, Investigation of the effect of sintering temperatures on the structural and magnetic properties of (Bi0.90Sm0.10Fe0.93Cr 0.07O3) ferrite, Mater. Chem. Phys. 303 (2023) 127790. https://doi.org/10.1016/j.matchemphys.2023.127790.

[3] M.R. Islam, M.S. Islam, M.A. Zubair, H.M. Usama, M.S. Azam, A. Sharif, Evidence of superparamagnetism and improved electrical properties in Ba and Ta co-doped BiFeO3 ceramics, J. Alloys Compd. 735 (2018) 2584–2596. https://doi.org/10.1016/j.jallcom.2017.11.323.

[4] S. Hait, S. Ghose, K. Mandal, Effect of Ba and Y co-doping on the structural and magneto-electric properties of BiFeO3 ceramic, J. Alloys Compd. 822 (2020) 153614. https://doi.org/10.1016/j.jallcom.2019.153614.

[5] M.S. Bernardo, Synthesis, microstructure and properties of BiFeO3-based multiferroic materials: A review, Bol. la Soc. Esp. Ceram. y Vidr. 53 (2014) 1–14. https://doi.org/10.3989/cyv.12014.

[6] D. Varshney, A. Kumar, K. Verma, Effect of A site and B site doping on structural, thermal, and dielectric properties of BiFeO3 ceramics, J. Alloys Compd. 509 (2011) 8421–8426. https://doi.org/10.1016/j.jallcom.2011.05.106.

[7] S.P. Balmuchu, P. Dobbidi, The effect of La doping on multiferroic BiFeO3 ceramic through structural, dielectric, magnetic, ferroelectric, and optical studies, Phys. B Condens. Matter. 638 (2022) 413937. https://doi.org/10.1016/j.physb.2022.413937.

[8] C. Wu, X. Qiu, W. Ge, L. Chen, C. Liu, et al., A co-doping strategy to achieve high energy storage performance in BiFeO3-based ceramics, Ceram. Int. 49 (2023) 29218–29228. https://doi.org/10.1016/j.ceramint.2023.06.208.

[9] T. Wang, S.H. Song, Q. Ma, M.L. Tan, J.J. Chen, Highly improved multiferroic properties of Sm and Nb co-doped BiFeO3 ceramics prepared by spark plasma sintering combined with sol-gel powders, J. Alloys Compd. 795 (2019) 60–68. https://doi.org/10.1016/j.jallcom.2019.04.327.

[10] P. Kum-onsa, N. Chanlek, P. Thongbai, P. Srepusharawoot, Effect of complex defects on the origin of giant dielectric properties of Mg2+–doped BiFeO3 ceramics prepared by a precipitation method,

Ceram. Int. 46 (2020) 25017–25023. https://doi.org/10.1016/j.ceramint.2020.06.287.
[11] S. Long, L. Liu, Z. Wang, X. Zhang, Enhanced ferroelectric and magnetoelectric properties of BiFeO3-based ceramics modified by SrTiO3, Ceram. Int. (2025). https://doi.org/10.1016/j.ceramint.2025.03.352.
[12] G. Qian, C. Zhu, L. Wang, Z. Tian, C. Yin, et al., Enhanced ferromagnetic, ferroelectric, and dielectric properties in BiFeO3-SrTiO3-Bi0.5Na0.5TiO3 ceramics, J. Electron. Mater. 46 (2017) 6717–6726. https://doi.org/10.1007/s11664-017-5689-0.
[13] H. Singh, K.L. Yadav, Structural, dielectric, vibrational and magnetic properties of Sm doped BiFeO3 multiferroic ceramics prepared by a rapid liquid phase sintering method, Ceram. Int. 41 (2015) 9285–9295. https://doi.org/10.1016/j.ceramint.2015.03.212.
[14] Y.P. Wang, L. Zhou, M.F. Zhang, X.Y. Chen, J.M. Liu, Z.G. Liu, Room-temperature saturated ferroelectric polarization in BiFeO3 ceramics synthesized by rapid liquid phase sintering, Appl. Phys. Lett. 84 (2004) 1731–1733. https://doi.org/10.1063/1.1667612.
[15] R. Montecillo, C.A. Chen, R.R. Chien, L.Y. Chen, C.S. Chen, et al., High-efficiency energy storage in BiFeO3 composite ceramics via BaO-TiO2-SiO2 glass modification, J. Eur. Ceram. Soc. 45 (2025) 117197. https://doi.org/10.1016/j.jeurceramsoc.2025.117197.
[16] Y.A. Chaudhari, A. Singh, C.M. Mahajan, P.P. Jagtap, E.M. Abuassaj, et al., Multiferroic properties in Zn and Ni co-doped BiFeO3 ceramics by solution combustion method (SCM), J. Magn. Magn. Mater. 347 (2013) 153–160. https://doi.org/10.1016/j.jmmm.2013.08.003.
[17] F. Azough, R. Freer, M. Thrall, R. Cernik, F. Tuna, D. Collison, Microstructure and properties of Co-, Ni-, Zn-, Nb- and W-modified multiferroic BiFeO3 ceramics, J. Eur. Ceram. Soc. 30 (2010) 727–736. https://doi.org/10.1016/j.jeurceramsoc.2009.09.016.
[18] X.L. Liang, J.Q. Dai, C.C. Zhang, Effect of (Zn, Mn) co-doping on the structure and ferroelectric properties of BiFeO3 thin films. Ceram. Int. 48 (2022) 6347–6355. https://doi.org/10.1016/j.ceramint.2021.11.177.
[19] J.H. Zhu, J.Q. Dai, J.W. Xu, X.Y. Li, Effect of Zn and Ti Co-doping on structure and electrical properties of BiFeO3 ceramics, Ceram. Int. 44 (2018) 9215–9220. https://doi.org/10.1016/j.ceramint.2018.02.131.
[20] R. Sharma, D. Basandrai, P. Sona Maji, R. Mukherjee, Tailoring of dielectric, ferroelectric, and optical properties of Bi0.99Nd0.1Fe2O3/ZnO nanocomposite at room temperature, Inorg. Chem. Commun. 165 (2024) 112526. https://doi.org/10.1016/j.inoche.2024.112526.
[21] T. Zheng, Y. Ding, J. Wu, Effects of oxide additives on structure and properties of bismuth ferrite-based ceramics, J. Mater. Sci.: Mater. Electron. 28 (2017) 11534–11542. https://doi.org/10.1007/s10854-017-6951-1.
[22] R. Hayati, A. Barzegar, Microstructure and electrical properties of lead free potassium sodium niobate piezoceramics with nano ZnO additive. Mater. Sci. Eng. B. 172 (2010) 121–126. https://doi.org/10.1016/j.mseb.2010.04.033.
[23] Y. Slimani, A. Selmi, E. Hannachi, M.A. Almessiere, A. Baykal, I. Ercan, Impact of ZnO addition on structural, morphological, optical, dielectric and electrical performances of BaTiO3 ceramics, J. Mater. Sci.: Mater. Electron. 30 (2019) 9520–9530. https://doi.org/10.1007/s10854-019-01284-2.
[24] K. Sarkar, H. Harsh, Z. Rahman, V. Kumar, Enhancing the structural, optical, magnetic and ferroelectric properties of perovskite BiFeO3 through metal substitution, Chem. Phys. Impact. 8 (2024) 100478. https://doi.org/10.1016/j.chphi.2024.100478.
[25] M.N. Rahaman, Ceramic Processing and Sintering, CRC press, (2017).
[26] S.A. Bhat, A. Rashid, M. Majeed, A.M. Tantray, A. Rani, et al., Enhanced magnetic, ferroelectric, and photocatalytic properties of Nd and Co doped bismuth ferrite (Bi1−xNdxFe1−yCoyO3) ceramics, Inorg. Chem. Commun. 170 (2024) 113148. https://doi.org/10.1016/j.inoche.2024.113148.
[27] N.T. Hien, N.D. Vinh, N.V. Dang, T.T. Trang, H.T. Van, et al., Structural transition and magnetic properties of Mn doped Bi0.88Sm0.12FeO3 ceramics, RSC Adv. 10 (2020) 11957–11965. https://doi.org/10.1039/D0RA01642J.